

# FORMATION OF RESONANT ATOMIC LINES DURING THERMONUCLEAR FLASHES ON NEUTRON STARS

PHILIP CHANG

Department of Physics, Broida Hall, University of California, Santa Barbara, CA 93106; pchang@physics.ucsb.edu

LARS BILDSTEN

Kavli Institute for Theoretical Physics and Department of Physics, Kohn Hall, University of California, Santa Barbara, CA 93106, USA;  
email: bildsten@kitp.ucsb.edu

AND

IRA WASSERMAN

Center for Radiophysics and Space Research, Cornell University, Ithaca, NY 14853; ira@astro.cornell.edu

*Draft version November 19, 2018*

## ABSTRACT

Motivated by the measurement of redshifted Fe H $\alpha$  lines during type I X-ray bursts on EXO 0748-676 (Cottam, Paerels & Mendez), we study the formation of atomic Fe lines above the photosphere of a bursting neutron star ( $k_B T_{\text{eff}} \approx 1 - 2$  keV). We discuss the effects of Stark broadening, resonant scattering and NLTE (level population) on the formation of hydrogenic Fe H $\alpha$ , Ly $\alpha$  and P $\alpha$  lines. From the observed equivalent width of the Fe H $\alpha$  line, we find an implied Fe column of  $1 - 3 \times 10^{20}$  cm<sup>-2</sup>, which is 3-10 times larger than the Fe column calculated from the accretion/spallation model of Bildsten, Chang & Paerels. We also estimate that the implied Fe column is about a factor of 2-3 larger than a uniform solar metallicity atmosphere. We discuss the effects of rotational broadening and find that the rotation rate of EXO 0748-676 must be slow, as confirmed by the recent measurement of a 45 Hz burst oscillation by Villarreal & Strohmayer. We also show that the Fe Ly $\alpha$  EW  $\approx 15$ -20 eV (redshifted 11-15 eV) and the P $\alpha$  EW  $\approx 4$ -7 eV (redshifted 3-5 eV) when the H $\alpha$  EW is 10 eV (redshifted 8 eV). The Ly $\alpha$  line is rotationally broadened to a depth of  $\approx 10\%$ , making it difficult to observe with *Chandra*. We also show that radiative levitation can likely support the Fe column needed to explain the line.

*Subject headings:* stars: abundances, surface – stars: neutron – X-rays: binaries, bursts – lines: formation

## 1. INTRODUCTION

The recent observation of gravitationally redshifted atomic transition lines during type I X-ray bursts on the low-mass X-ray binary, EXO 0748-676 (Cottam, Paerels & Mendez 2002, hereafter CPM) opens a new window on neutron star (NS) structure. Using 335 ks of XMM-Newton observations during its calibration and commissioning phase, CPM collected 3.2 ks of Type I bursts which was split into a high temperature part ( $k_B T_{\text{BB}} \approx 1.8$  keV) and a low temperature part ( $k_B T_{\text{BB}} < 1.5$  keV). In the high temperature part they identified the H $\alpha$  ( $n = 2 \rightarrow 3$ ) transition of hydrogenic Fe with a redshift of  $z=0.35$ . The same transition was identified for He-like Fe with the same redshift in the low temperature part. Though this is not the first claim of an absorption feature during type I X-ray bursts, previous Tenma and EXOSAT observations of a 4.1 keV absorption feature on 2S 1636-536 (Waki et al. 1984; Turner & Breedon 1984), EXO 1747-214 (Magnier et al. 1989) and X1608-52 (Nakamura, Inoue & Tanaka 1988) were never confirmed with more sensitive instruments. CPM's observation is unique in that two lines in distinct states of the type I burst with the same redshift were observed, implying that we are seeing the NS surface.

In our previous work (Bildsten, Chang & Paerels 2003, hereafter BCP), we explained how Fe can be present above the accreting NS photosphere. The larger entropy

of the photosphere forbids convective mixing from the deeper burning regions (Joss 1977), making it unlikely that Fe is dredged up. In addition, the strong surface gravity rapidly depletes Fe from the upper atmosphere via sedimentation<sup>1</sup>. However, continual accretion during the burst at fairly modest rates ( $\dot{M} > 10^{-12} M_{\odot} \text{ yr}^{-1}$ ) can overcome Fe sedimentation. For EXO 0748-676, the persistent flux implies  $\dot{M} > 2 \times 10^{-10} M_{\odot} \text{ yr}^{-1}$  (Gottwald et al. 1986; CPM) and the sub-Eddington burst luminosity is unlikely to halt the accretion flow (see observations of GX 17+2; Kuulkers et al. 2002).

If accretion is the source of the Fe that generates the absorption line, then accretion must be spread over a large fraction of the star. Since the NS surface is inside the last stable orbit for the implied radius of  $R = 4.4GM/c^2$  (CPM), the protons may reach the NS surface with a kinetic energy of  $\approx 200 - 300$  MeV/nucleon, and decelerate via Coulomb scattering (Zel'dovich & Shakura 1969). This filters ions by their charge and mass, stopping incident Fe above the photosphere at a column of  $\approx 1 \text{ g cm}^{-2}$  (Bildsten, Salpeter & Wasserman 1992). The Fe remains there until it is either destroyed by incident protons (for  $\dot{M} > 10^{-13} M_{\odot} \text{ yr}^{-1}$ ) or sediments out. The deposition and nuclear destruction of Fe both

<sup>1</sup> Radiative levitation is a possible mechanism by which the Fe is suspended (BCP), an issue we will address in § 3.3.

depend linearly on  $\dot{M}$  and hence the steady state Fe column is independent of  $\dot{M}$  when nuclear destruction dominates. For accretion of solar metallicity material,  $N_{\text{Fe}} \approx 3.4 \times 10^{19} \text{ cm}^{-2}$  (BCP). While this Fe column is similar to a uniformly abundant solar metallicity atmosphere ( $N_{\text{Fe}} \approx 5 \times 10^{19} \text{ cm}^{-2}$ ), the accretion/spallation scenario also predicts a plethora of elements with  $Z < 26$  produced by proton spallation of Fe (BCP, Table 1).

In this paper, we discuss the physics of line transfer through a thin Fe layer above the continuum photosphere. Previous theoretical work on the formation of spectral features focused on the Fe Ly $\alpha$  line and edge (Foster et al. 1987; Day, Fabian & Ross 1992). However, these calculations presumed LTE and uniform abundance. In § 2 we show that LTE is a poor assumption as the radiation field dominates the level population and ionization balance (London, Taam & Howard 1986; BCP). We also discuss the line broadening physics and show that Stark broadening dominates for Fe H $\alpha$ . We calculate in § 3 the Fe column needed to produce the observed H $\alpha$  line and compare it to the Fe column from accretion/spallation. We also estimate the equivalent width of the resulting Ly $\alpha$  and P $\alpha$  transition, and constrain the rotation rate of the NS from the observed linewidth. We close by estimating the Fe column that might be sustained by radiative levitation, and summarize our results in § 4.

## 2. MODEL ATMOSPHERES

We model the thin Fe line forming region as a one-zone scattering layer (Mihalas 1978) at fixed temperature and density that is illuminated from below by the continuum photosphere (see Figure 1). We consider radiation and gas temperatures of  $k_B T_g \approx k_B T_{\text{eff}} \approx 1 - 2 \text{ keV}$ , in which case the atmospheric microphysics is simplified. The continuum opacity,  $\kappa_{\text{cont}} = \kappa_{\text{abs}} + \kappa_{\text{Th}}$ , where  $\kappa_{\text{abs}}$  is the absorption opacity (mostly free-free) and  $\kappa_{\text{Th}}$  is the Thomson scattering opacity, is dominated by electron scattering. Bound-free transitions are suppressed since most atoms are fully ionized (Pavlov, Shibanov & Zavlin 1991; London et al. 1986). We do not consider the global problem of the thermal spectra from a bursting NS (for a review see Lewin, Van Paradijs & Taam 1993 and references therein), but rather the simplified problem of line transport in the Fe layer. The spectra from a bursting neutron star, whose opacity is scattering dominated, is expected to be non-Planckian (Zeldovich & Shakura 1969; Castor 1974; Madej 1974; van Paradijs 1982). For our purposes, we take the color correction given by Madej, Joss & Rozanska (2004) (also see Madej 1991) to relate the observed color temperature to the effective temperature. The effect of the color correction is nearly offset by the measured redshift correction. Hence the observed color temperature *at infinity* is roughly the effective temperature *at the surface*. For the sake of simplicity, we approximate the continuum flux with a blackbody at the effective temperature. However, we will discuss the effect of the spectral shape of the continuum flux on our results in § 3.1.

We assume that the continuum is formed below the line forming region and is freely streaming. The equation of radiative transfer is then (Mihalas 1978)

$$\mu \frac{\partial I_\nu}{\partial y} = -(\kappa_{\text{abs}} + \kappa_{\text{Th}} + \psi_l \phi_\nu) I_\nu + \kappa_{\text{abs}} B_\nu + \kappa_{\text{Th}} J_\nu$$

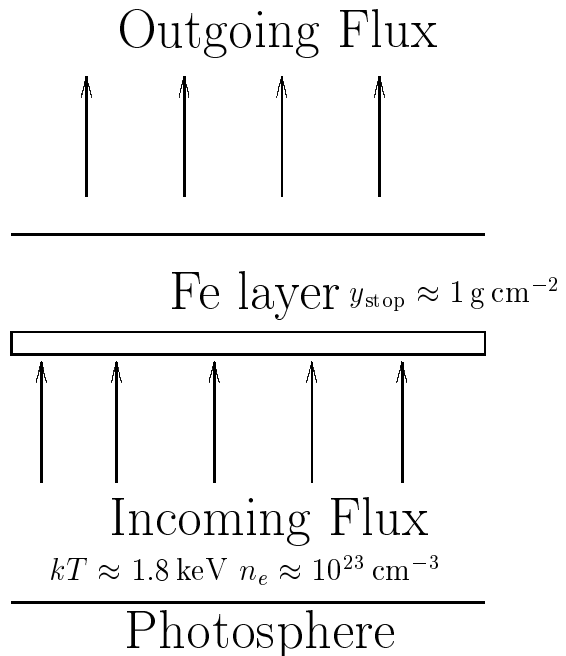


FIG. 1.— Schematic model of the line forming region in a NS atmosphere during a Type I burst.

$$+\epsilon \psi_l \phi_\nu B_\nu + (1 - \epsilon) \psi_l \int R(\nu, \nu') J_\nu d\nu', \quad (1)$$

where  $I_\nu$  is the frequency and angle dependent specific intensity,  $J_\nu = (1/2) \int I_\nu d\mu$  is the angle-average mean intensity,  $B_\nu$  is the Planck function,  $\psi_l$  is the line opacity properly normalized,  $\epsilon = \kappa_{\text{abs}}/\kappa_{\text{tot}}$  is the absorbed fraction, where  $\kappa_{\text{tot}} = \kappa_{\text{cont}} + \psi_l$ ,  $\phi$  is the line profile distribution and is determined by the physics of § 2.1, and  $R(\nu, \nu')$  is the redistribution function. The coordinate  $y$  measures the column from the base of the scattering layer.

### 2.1. Line Broadening Physics

We begin by discussing the line broadening physics. The number density of fully ionized H at the photosphere is

$$n_p \approx 2 \times 10^{23} \left( \frac{1 \text{ keV}}{k_B T_g} \right) \left( \frac{g}{3 \times 10^{14} \text{ cm s}^{-2}} \right) \text{ cm}^{-3}, \quad (2)$$

where  $g$  is the surface gravity. It is sufficiently dense so that the intrinsic broadening of the hydrogenic Fe H $\alpha$  line is dominated by the linear Stark effect (Paerels 1997). The linear Stark effect is only relevant for hydrogenic atoms and breaks down for multi-electron atoms where the degeneracies of opposite parity states are broken (Bethe & Salpeter 1957). The distribution of the electric microfields is given by the Holtsmark distribution (Mihalas 1978; also see Potekhin, Chabrier, & Gilles 2002) and the characteristic scale is given from interactions with neighboring protons,  $E = e/r_0^2$ , where  $r_0 = (4\pi n_p/3)^{-1/3} = 5 \times 10^{-9} \rho^{-1/3} \text{ cm}$  is the mean ion spacing and  $\rho = n_p m_p$  is the density. Hence the scale of Stark broadening is

$$\Delta E_{\text{Stark}} = h \Delta \nu_{\text{Stark}} \approx \frac{\hbar^2 n^2}{m_e Z r_0^2}$$

$$\approx 1.5 Z_{26}^{-1} \left( \frac{n_p}{10^{23} \text{ cm}^{-3}} \right)^{2/3} \left( \frac{n}{3} \right)^2 \text{ eV}, \quad (3)$$

for the  $\text{H}\alpha$  line, 0.6 eV for the  $\text{Ly}\alpha$  line, and 2.7 eV for the  $\text{P}\alpha$  line, where  $Z_{26} = Z/26$ . Note that we have chosen the upper state because of the strong dependence on  $n$ . The scale of thermal Doppler broadening is

$$\begin{aligned} \Delta E_{\text{th}} &= h\Delta\nu_{\text{th}} = \left( \frac{2k_B T_g}{Am_p c^2} \right)^{1/2} E_{\text{tran}} \\ &\approx 0.25 \left( \frac{k_B T_g}{1 \text{ keV}} \right)^{1/2} \left( \frac{A}{56} \right)^{-1/2} \left( \frac{E_{\text{tran}}}{1.276 \text{ keV}} \right) \text{ eV} \end{aligned} \quad (4)$$

where  $E_{\text{tran}}$  is the line energy, scaled to the  $\text{H}\alpha$  transition and  $A_{56} = A/56$ . For  $\text{Ly}\alpha$  and  $\text{P}\alpha$ ,  $\Delta E_{\text{th}} \approx 1.4$  eV and  $\Delta E_{\text{th}} \approx 0.087$  eV respectively. Stark broadening dominates the  $\text{H}\alpha$  line and  $\text{P}\alpha$ , but thermal Doppler broadening dominates the  $\text{Ly}\alpha$  line. The relative strength of Stark and thermal Doppler broadening scales like

$$\begin{aligned} \lambda \equiv \frac{\Delta\nu_{\text{th}}}{\Delta\nu_{\text{Stark}}} &\approx 11 Z_{26}^3 A_{26}^{-1/2} \left( \frac{k_B T_g}{1 \text{ keV}} \right)^{1/2} \\ &\quad \left( \frac{n_p}{10^{23} \text{ cm}^{-3}} \right)^{-2/3} \frac{|n^{-2} - n'^{-2}|}{n^2}, \end{aligned} \quad (5)$$

where  $n$  is the upper state and  $n'$  is the lower state. Note the dependence on  $n$  and  $n'$ . Depending on the values of  $n$  and  $n'$ , the relative strengths of the two broadening mechanisms can vary tremendously. For instance for the  $\text{H}\alpha$  transition,  $\lambda \approx 0.17$ , while for the  $\text{Ly}\alpha$  and  $\text{P}\alpha$  transitions  $\lambda \approx 2$  and  $\approx 0.033$  respectively.

The timescale of changes in electric microfields is  $\tau_{\text{El}} = r_0/v_{\text{th}}$ , where  $v_{\text{th}} = \sqrt{2k_B T_g/m_p}$  is the thermal speed of the perturbing protons. At photospheric temperatures and densities, this gives  $\tau_{\text{El}} \approx 7 \times 10^{-16} \text{ s} (k_B T_g/1 \text{ keV})^{-1/2} (n_p/10^{23} \text{ cm}^{-3})^{-1/3}$ , much smaller than the  $n = 3 \rightarrow 2$  radiative deexcitation timescale of  $3.1 \times 10^{-14} \text{ s}$ . Since the electric field changes during the time in which the atom absorbs and re-emits a photon, the energy of the two  $\text{H}\alpha$  photons are uncorrelated. With this in mind, we can assume *complete redistribution*, greatly simplifying the line transport calculation.

The final broadening profile is a convolution of Stark and thermal Doppler broadening. In Figure 2, we show these profiles for various values of  $\lambda$ . Asymptotically, the distribution approaches the power law  $\propto (\Delta\nu/\Delta\nu_{\text{Stark}})^{-2.5}$ , expected for the Holtmark distribution (Mihalas 1978). For  $\lambda \gg 1$ , we recover the thermal Doppler profile. For  $\lambda \ll 1$ , we approach the Holtmark distribution. Note that for small values of  $\lambda$ , there is a severe deficit at zero shift because this shift corresponds to perfect symmetry in the proton distribution. In fact for  $\lambda = 0$ , the probability of a zero shift goes precisely to zero. The effect of thermal Doppler broadening is to fill in the distribution near zero (see Figure 2). The deficit near zero shift yields an emission-like feature there, which must be interpreted as reduced scattering. This is similar to the ‘‘ghost of  $\text{Ly}\alpha$ ’’ where reduced scattering in the line contributes to an emission-like feature in the spectra of broad absorption line (BAL) quasars (Arav 1996).

## 2.2. NLTE Effects

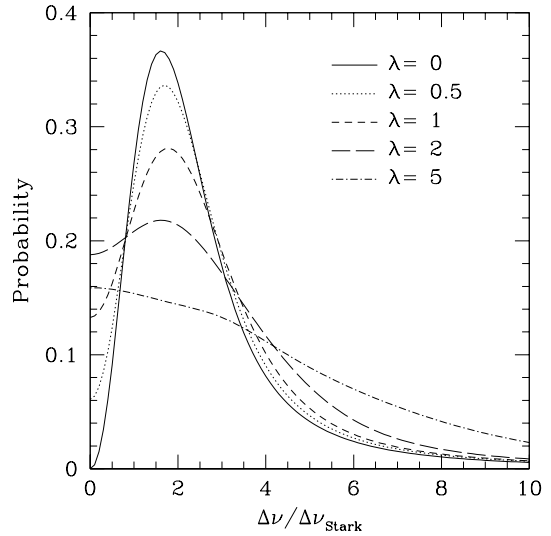


FIG. 2.— Distribution of frequency shifts due to a combination of thermal Doppler (Voigt) and Stark shifts (Holtmark) at various relative strengths of each. The x-axis is given in units of  $\Delta\nu_{\text{Stark}}$  and the relative strengths of each distribution is given by  $\lambda = \Delta\nu_{\text{th}}/\Delta\nu_{\text{Stark}}$ . The limits of  $\lambda = 0$  and  $\lambda \gg 1$  gives the Holtmark distribution and the Voigt profile respectively.

We now show that the atomic level populations in the photospheres of bursting neutron stars are not expected to be in LTE (London et al. 1986, BCP). For simplicity we only consider a two-level system. The rate equations for the density of upper ( $n_u$ ) and lower ( $n_l$ ) states are then,

$$0 = n_l [C_{lu} + B_{lu}J(E_{lu})] - n_u [C_{ul} + A_{ul} + B_{ul}J(E_{lu})], \quad (6)$$

where  $C_{lu,ul}$  are the collisional rates from the lower to upper state and vice versa,  $A$  and  $B$  are the Einstein coefficients,  $E_{lu}$  is the energy of the transition and  $J$  is the mean radiation intensity at that energy. We take the dipole approximation from Jefferies (1962) for optically allowed transitions for the collisional rates:

$$\begin{aligned} C_{lu} &= 5.5 \times 10^{12} \left( \frac{E_{lu}}{k_B T_g} \right)^{-1.68} \exp \left( -\frac{E_{lu}}{k_B T_g} \right) \\ &\quad \left( \frac{k_B T_g}{1 \text{ keV}} \right)^{-1.5} \left( \frac{n_e}{10^{23} \text{ cm}^{-3}} \right) f_{lu} \text{ s}^{-1}, \end{aligned} \quad (7)$$

where  $f_{lu}$  is the oscillator strength for the transition. Putting this all together, we have  $C_{lu} \approx 2.2 \times 10^9 \text{ s}^{-1}$  for the  $n = 1 \rightarrow 2$  transition and  $1.3 \times 10^{12} \text{ s}^{-1}$  for the  $n = 2 \rightarrow 3$  transition at  $k_B T_g = 1.8 \text{ keV}$ . If we compare this to the radiative excitation/deexcitation rates in the same conditions, we find that  $B_{lu}J(E_{lu}) = 7 \times 10^{13} \text{ s}^{-1}$  for the  $n = 1 \rightarrow 2$  transition and  $R_{lu} = 7 \times 10^{12} \text{ s}^{-1}$ , easily exceeding the collisional rates for the  $n = 2 \rightarrow 3$  transition at a radiation temperature of  $k_B T_{\text{eff}} = 1.8 \text{ keV}$ .

Having radiative rates exceed collisional rates is not the only prerequisite to break LTE. If the radiation field were isotropic and Planckian, we would recover the Boltzmann distribution for the level populations where the relevant temperature setting the level populations is that of the radiation. Hence to break LTE, we require the radiation field to be either non-Planckian, anisotropic or both. This is indeed the case above the photosphere where the

radiation field is free-streaming and the source function deviates from Planckian due to the nature of scattering dominated atmospheres (Mihalas 1978). Therefore, to successfully model the spectral line formation, we must solve the equations of radiative transfer and statistical equilibrium simultaneously.

### 3. LINE FORMATION CALCULATIONS

We rewrite equation (1) by defining the flux  $F_\nu = (1/2) \int \mu I_\nu d\mu$  and  $K_\nu = (1/2) \int \mu^2 I_\nu d\mu$ . Integrating equation (1) over  $d\mu$  and  $\mu d\mu$  we find (Mihalas 1978),

$$\frac{\partial F_\nu}{\partial \tau_\nu} = -J_\nu + (1 + \beta_\nu)^{-1} [(1 - \rho + \epsilon \beta_\nu) B_\nu + \rho J_\nu + (1 - \epsilon) \beta_\nu \int R(\nu, \nu') J_{\nu'} d\nu'], \quad (8)$$

$$\frac{\partial K_\nu}{\partial \tau_\nu} = -F_\nu, \quad (9)$$

where  $d\tau_\nu = (\kappa_{\text{abs}} + \kappa_{\text{Th}} + \psi_I \phi_\nu) dy$ ,  $\rho = \kappa_{\text{Th}} / (\kappa_{\text{abs}} + \kappa_{\text{Th}})$  and  $\beta_\nu = \psi_I \phi_\nu / (\kappa_{\text{abs}} + \kappa_{\text{Th}})$ . Note that  $\tau_\nu$  is defined from the base of the scattering layer. If we define the variable Eddington factor as  $f_\nu = K_\nu / J_\nu$ , we can write equation (9) as

$$\frac{\partial^2 f_\nu J_\nu}{\partial \tau_\nu^2} = J_\nu - (1 + \beta_\nu)^{-1} [(1 - \rho + \epsilon \beta_\nu) B_\nu + \rho J_\nu + (1 - \epsilon) \beta_\nu \int R(\nu, \nu') J_{\nu'} d\nu'] \quad (10)$$

Equation (10) is a generalization of Harrington's (1973) equation including the use of variable Eddington factors.

We solve equation (10) with a standard methodology (Mihalas 1978). Following the nomenclature of Mihalas (1978) we define a symmetric and antisymmetric average for the intensity

$$u_\nu(\tau_\nu, |\mu|) = \frac{1}{2} [I_\nu(\tau_\nu, |\mu|) + I_\nu(\tau_\nu, -|\mu|)] \quad (11)$$

$$v_\nu(\tau_\nu, |\mu|) = \frac{1}{2} [I_\nu(\tau_\nu, |\mu|) - I_\nu(\tau_\nu, -|\mu|)], \quad (12)$$

which combined with the equation of radiative transfer (eq.[1]) yields

$$|\mu| \frac{\partial v_\nu}{\partial \tau_\nu} = -u_\nu + S_\nu, \quad (13)$$

$$|\mu| \frac{\partial u_\nu}{\partial \tau_\nu} = -v_\nu, \quad (14)$$

where

$$S_\nu = (1 + \beta_\nu)^{-1} [(1 - \rho + \epsilon \beta_\nu) B_\nu + \rho J_\nu + (1 - \epsilon) \beta_\nu \int R(\nu, \nu') J_{\nu'} d\nu'] \quad (15)$$

is the source function. To solve this system of equations, we take an initial guess for the variable Eddington factor,  $f_\nu$ , and assume an initial input  $I_\nu$  at the bottom of the scattering layer that is isotropic in the outward half space ( $\mu \geq 0$ ). We then solve for  $J_\nu$  in equation (10). We compute  $S_\nu$  given  $J_\nu$  and solve for  $u_\nu$  and  $v_\nu$  in equation (13). With  $u_\nu$  and  $v_\nu$  in hand, we compute,  $I_\nu$ ,  $F_\nu$ , and  $K_\nu$ , compute a new  $f_\nu$  and iterate to convergence.

Since the atmosphere is in NLTE and scattering dominated, we must simultaneously solve the equations

of radiative transfer (eq.[1]) and statistical equilibrium (eq.[6]). For simplicity, we assume a two-level atom and calculate the level populations between the two states (in the case of H $\alpha$ , the two states are the n=2 and n=3 states; for Ly $\alpha$ , n=1 and n=2; for P $\alpha$ , n=3 and n=4) fixing the sum of the two states. We iteratively solve the radiative transfer equation (eq.[1]) and use the computed mean intensities to solve for statistical equilibrium (eq.[6]); i.e.  $\Lambda$  iteration. We define convergence when the mean intensity varied by less than  $\delta J/J < 10^{-3}$ , which was typically achieved in 3-5 iterations.

#### 3.1. Line Profile and Equivalent Width

We solve the thin scattering layer illustrated by Figure 1 with the above technique. However, before we continue, we review the analytic result of a specific case of scattering dominated atmosphere known as Schuster's law (Schuster 1905). Assuming that line opacity is dominant ( $\beta_\nu \gg 1$ ), the absorbed fraction is small ( $\epsilon \rightarrow 0$ ), and the scattering is coherent ( $R(\nu', \nu) = \delta_{\nu', \nu}$ ), equation (10) becomes

$$\frac{\partial^2 f_\nu J_\nu}{\partial \tau_\nu^2} = 0. \quad (16)$$

Solving this equation, we find  $f_\nu J_\nu = A_\nu \tau_\nu + B_\nu$ , where  $A_\nu$  and  $B_\nu$  are constants. From equation (9), we also find  $F_\nu = f_\nu A_\nu$ .

We now make some further approximations to determine  $A_\nu$  and  $B_\nu$ . We assume the Eddington approximation everywhere so that  $f_\nu = 1/3$  (Rybicki & Lightman 1979). We also assume the two stream approximation, which breaks the radiation field into one outgoing stream ( $I_\nu^+ = I_\nu(\tau_\nu, |\mu|)$ ) and one incoming stream ( $I_\nu^- = I_\nu(\tau_\nu, -|\mu|)$ ). Consistency with the Eddington approximation demands  $|\mu| = 1/\sqrt{3}$  (Rybicki & Lightman 1979). The boundary conditions are that the incoming flux at the surface is zero,  $I_\nu(\tau_\nu = \tau_\nu^{\text{tot}}, \mu = -1/\sqrt{3}) = 0$ , where  $\tau_\nu^{\text{tot}}$  is the total optical depth of the scattering layer at frequency  $\nu$  and that below the line forming region, the incident intensity is fixed at some value typical for Type I bursts ( $I_\nu(\tau_\nu = 0, \mu = 1/\sqrt{3}) = I_{\text{inc}}$ ). Per frequency the optical depth of the slab is given by  $\tau_\nu^{\text{tot}} = \tau_0^{\text{tot}} \phi(\nu)$ , where  $\tau_0^{\text{tot}}$  is the normalization of the optical depth and is given by

$$\begin{aligned} \tau_0^{\text{tot}} &= N_{\text{Fe}, n=2} \sigma_{0,23} \\ &\approx 6.1 \left( \frac{N_{\text{Fe}, n=2}}{10^{17} \text{ cm}^{-2}} \right) \left( \frac{n_p}{10^{23} \text{ cm}^{-3}} \right) \left( \frac{Z}{26} \right)^{-1}, \end{aligned} \quad (17)$$

where  $\sigma_{0,23} = \pi e^2 f_{23} / (m_e c \Delta \nu_{\text{Stark}})$  is the cross section at line center. In the two-stream approximation, our definitions for the mean intensity and the flux become

$$J_\nu = \frac{1}{2} (I_\nu^+ + I_\nu^-) \quad (18)$$

$$F_\nu = \frac{1}{2\sqrt{3}} (I_\nu^+ - I_\nu^-) \quad (19)$$

and hence solving for  $A_\nu$  and  $B_\nu$ , we find

$$I_{\text{trans}} = I_{\text{inc}} \frac{2}{\sqrt{3} \tau_\nu^{\text{tot}} + 2}, \quad (20)$$

where  $I_{\text{trans}} = I_\nu(\tau_\nu = \tau_\nu^{\text{tot}}, \mu = 1/\sqrt{3})$  is the transmitted intensity. Equation (20) is known as Schuster's

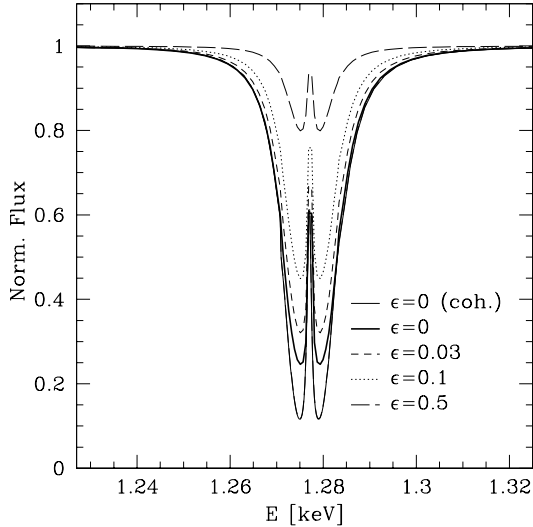


FIG. 3.— Hydrogenic Fe H $\alpha$  line profiles of various values of  $\epsilon$  in the line at the NS surface. For the background we take  $\tau_0^{\text{tot}} = 100$ ,  $k_B T_{\text{eff}} = 1.8$  keV and  $n_p = 10^{23}$  cm $^{-3}$ . The numerical calculation of two stream approximation and exact analytic result (eq.[20]) are indistinguishable and are represented by the thin-solid line. The full numerical results properly angle averaged for complete redistribution are represented by the other curves for various values of the absorption ratio  $\epsilon$ . The difference between the thin-solid line and the thick-solid line are due to the departures of the two-stream approximation compared to the full angle-averaged solution and coherent scattering compared to complete redistribution. The difference between the other curves are due to different values of  $\epsilon$ .

law. Note that at large  $\tau_\nu^{\text{tot}}$ , the specific intensity scales with  $1/\tau_\nu^{\text{tot}}$  unlike the absorption dominated case where  $I_\nu \rightarrow B_\nu$  at large  $\tau_\nu^{\text{tot}}$ . This difference in scaling with optical depth between a scattering dominated atmosphere and an absorption dominated atmosphere is the key to understanding the nature of the Fe H $\alpha$  line.

We compare the flux from our exact numerical calculations with Schuster's law (eq.[20]) in Figure 3. For simplicity of the discussion, we take a simple model of a hydrogenic atom whose energy levels are defined by  $E_n = -13.6 Z^2 n^{-2}$  eV, which gives the energy of the Fe H $\alpha$  transition of 1.2769 keV. We will consider the fully relativistic atom with the complications of fine structure splitting later. We take  $\tau_0^{\text{tot}} = 100$ ,  $k_B T_{\text{eff}} = 1.8$  keV and  $n_p = 10^{23}$  cm $^{-3}$  for these models. Our numerical calculation for coherent scattering in the two-stream approximation and Schuster's law are indistinguishable and are both represented by the thin-solid line. This confirms the accuracy of our numerical treatment with the exact analytic result. The other calculations represent the full numerical solutions with *complete redistribution* with the variable Eddington factor,  $f_\nu$ , computed self-consistently. These curves are computed with 10 angular points, 100 frequency points and 100 depth points at various values of the absorption coefficient  $\epsilon$ . The difference between the thick-solid line and the thin-solid line is due to differences between coherent scattering and complete redistribution and the nature of the two-stream approximation which fixes  $f_\nu = 1/3$  at every point compared to the full self-consistent calculation. Note the emission-like feature at line center, which is due to the deficit near zero shift discussed in § 2.1.

Now that we have established the effectiveness of our numerical code, we discuss the nature of the hydrogenic Fe Ly $\alpha$ , H $\alpha$  and P $\alpha$  lines. Since we have limited our study to two-level atomic systems, the relevant transitions starting from the 1s ground state are  $1s \rightleftharpoons 2p$ ,  $2p \rightleftharpoons 3d$  and  $3d \rightleftharpoons 4f$ . The fine structure splitting of these transitions significantly complicates the line structure<sup>2</sup>. Due to fine structure splitting the energy levels of an hydrogenic atom are

$$E_{n,j} = -13.6 \frac{Z^2}{n^2} \left[ 1 + \frac{(\alpha Z)^2}{n} \left( \frac{1}{k} - \frac{3}{4n} \right) \right] \text{ eV}, \quad (21)$$

where  $j$  is the total angular momentum quantum number,

$$k = \begin{cases} l & \text{if } j = l - \frac{1}{2}, \\ l + 1 & \text{if } j = l + \frac{1}{2}, \end{cases} \quad (22)$$

$l$  is the orbital quantum number, and  $\alpha$  is the fine structure constant. The Ly $\alpha$   $1s \rightleftharpoons 2p$  transition is fine structure split into two lines with relative line intensities of 2:1 with energies of 6.9728 keV and 6.9521 keV, a difference of 20.7 eV. The H $\alpha$   $2p \rightleftharpoons 3d$  transition is split into three lines with relative line intensities of 9:1:5 and energies of 1.2811 keV, 1.2790 keV, and 1.2997 keV. Taking the energy of the strongest line to be the centroid, the splitting of the levels are 0, -2.1, 18.6 eV (Bethe & Salpeter 1957). The size of the splitting is comparable to the EW and the FWHM of the observed line. Finally the P $\alpha$   $3d \rightleftharpoons 4f$  transition is split into three lines with intensities 20:1:14 and energy differences of 0, -0.43, 1.61 eV. These splittings are smaller than the effect of Stark broadening, so that their effect on the line profile is small.

We illustrate the line profile with fine structure splitting in Figure 4. We also turn on statistical equilibrium so that from an initial state where the initial population of the two-level atom was assumed to be in the  $n=2$  state (with an optical depth normalization of  $\tau_0^{\text{tot}} = 100$ ), we simultaneously solve radiative transfer and statistical equilibrium. Since the opacity is dominated by line itself, the absorbed fraction is determined from the ratio of the collisional rate to the total transition rates ( $\epsilon \equiv \kappa_{\text{abs}}/\kappa_{\text{tot}} \approx C_{lu}/(R_{lu} + C_{lu})$ ). In statistical equilibrium,  $\epsilon$  relaxes to a small value of 0.033, typical of a scattering dominated atmosphere. This line profile represents the complete solution to the spectra from the resonant scattering layer. Note that the triplet structure of the fine structure lines is reduced to a doublet because Stark broadening is so large.

The line's equivalent width (EW) is the proportional deficit and is defined as

$$EW \equiv \int \left( 1 - \frac{F_\nu^{\text{line}}}{F_\nu^{\text{cont.}}} \right) d\nu. \quad (23)$$

Though rotation will modify the line profile, it conserves equivalent width (Gray 1992) to first order in  $\Omega R/c$ , where  $\Omega$  is the angular rotation rate. In Figure 5, we show the fractional equivalent width, defined as the equivalent width in wavelength units over the line center wavelength, as a function of the Fe column in the  $n = 2$  state for  $n_p = 5.2 \times 10^{22}$  cm $^{-3}$  (dotted line) and  $n_p = 10^{23}$  cm $^{-3}$  (solid line), corresponding to the

<sup>2</sup> We thank Rashid Sunyaev for raising this important issue.

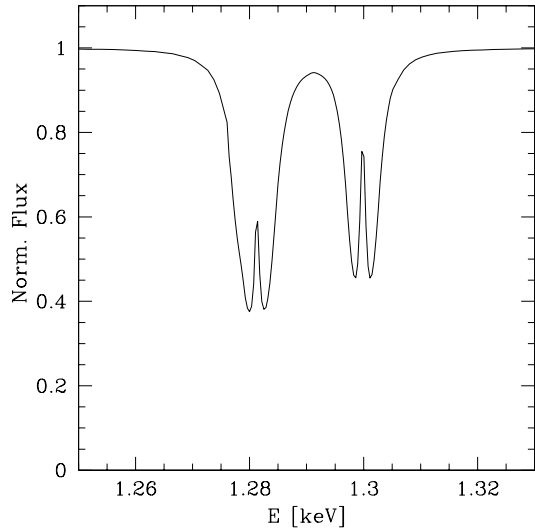


FIG. 4.— Hydrogenic Fe H $\alpha$  line profiles with fine structure splitting. We take the same background as Figure 3 ( $k_B T_{\text{eff}} = 1.8$  keV and  $n_p = 10^{23}$  cm $^{-3}$ ). We also simultaneously solve statistical equilibrium assuming an initial two-level system with everything in the  $n=2$  state with an optical depth normalization of  $\tau_0^{\text{tot}} = 100$ . With these parameters, statistical equilibrium gives  $\epsilon \approx 0.033$ .

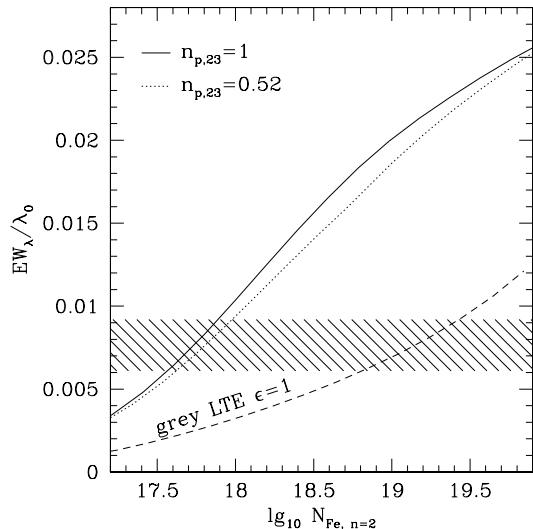


FIG. 5.— Fractional Equivalent width as a function of the Fe column in the  $n=2$  state for two different proton densities of  $n_p = 5.2 \times 10^{22}$  cm $^{-3}$  (dotted line) and  $n_p = 10^{23}$  cm $^{-3}$  (solid line) at  $k_B T_{\text{eff}} = 1.8$  keV. We show the observed EW as a banded region and the intersection of these lines with the banded region indicates the  $n=2$  Fe column needed. We also present an extremal LTE calculation (dashed line) where  $A_0 \approx 0.2$  (BCP) for comparison.

Coulomb stopping density for radial infall and the  $\tau \approx 1$  surface (approximating a solar metallicity atmosphere) for a radiation temperature of  $k_B T_{\text{eff}} = 1.8$  keV. We also show the observed EW (CPM). The scattering dominated calculations imply  $N_{\text{Fe}, n=2} \approx 5 \times 10^{17}$  cm $^{-2}$ . We also plot an extremal grey atmosphere model in perfect LTE ( $\epsilon = 1$ ) for comparison. The LTE calculation requires a much larger  $N_{\text{Fe}, n=2}$  and highlights how poor the LTE calculation fares compared to the full resonant calculation.

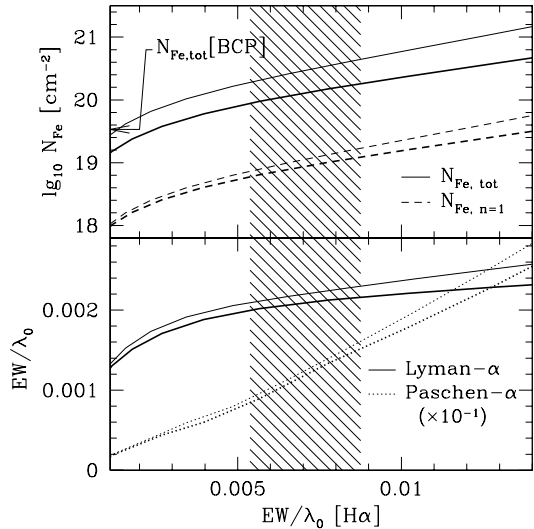


FIG. 6.—  $N_{\text{Fe}, n=1}$ ,  $N_{\text{Fe}}$ ,  $\text{EW}_{\text{Ly}\alpha}$ , and  $\text{EW}_{\text{P}\alpha}$  as a function of total  $\text{EW}_{\text{H}\alpha}$  for parameters  $n_p = 5.2 \times 10^{22}$  cm $^{-3}$  (thin lines),  $n_p = 10^{23}$  cm $^{-3}$  (thick lines) and  $k_B T_{\text{eff}} = 1.8$  keV. The banded region represents the observed EW and the intersection of these lines with the banded region indicates the Fe column (upper plot) needed in the hydrogenic ground state (dashed lines) and total Fe (solid lines) and the predicted EW in the Ly $\alpha$  line (solid lines; lower plot) and P $\alpha$  line (dotted lines; lower plot). The P $\alpha$  values have been divided by 10 so that they may fit on the same plot.

We calculate a grid of models for the Ly $\alpha$ , H $\alpha$  and P $\alpha$  transitions to relate the equivalent widths and level populations in each transition to one another. We estimate the total  $N_{\text{Fe}}$  to that in the  $n=1$  state via Saha equilibrium. Since the radiation field drives ionization, we expect our results from Saha equilibrium will give a *lower* bound on  $N_{\text{Fe}}$ . We relate  $\text{EW}_{\text{H}\alpha}$ ,  $N_{\text{Fe}, n=1}$ ,  $N_{\text{Fe}}$ ,  $\text{EW}_{\text{Ly}\alpha}$  and  $\text{EW}_{\text{P}\alpha}$  in Figure 6 at two different proton densities:  $n_p = 5.2 \times 10^{22}$  cm $^{-3}$  (Fe stopping layer; dotted line) and  $n_p = 10^{23}$  cm $^{-3}$  (solid line). The larger proton density is indicative of what would happen in a uniform metallicity atmosphere. The observed Fe H $\alpha$  EW gives an implied column of  $N_{\text{Fe}, n=1} \approx 1 - 2 \times 10^{19}$  cm $^{-2}$  if all the Fe is concentrated in the Fe stopping layer. Saha equilibrium then implies a total Fe column of  $N_{\text{Fe}} = 3 - 6 \times 10^{20}$  cm $^{-2}$  at the Fe stopping layer, a factor of  $\approx 10$  higher than the solar metallicity accretion/spallation scenario. For the larger proton density ( $n_p = 10^{23}$  cm $^{-3}$ ), the implied Fe column is  $\approx 10^{20}$  cm $^{-2}$ , a factor of two larger than that implied by a uniform solar metallicity photosphere. Since ionization balance is likely given by the radiation field (London et al. 1986), the *true*  $N_{\text{Fe}}$  is likely even higher for both these scenarios. We also estimate that our implied  $N_{\text{Fe}, n=1}$  gives an  $\text{EW}_{\text{Ly}\alpha} \approx 15 - 20$  eV (redshifted 11-15 eV). Though this is larger than  $\text{EW}_{\text{H}\alpha}$ , rotational broadening has a large impact on its detectability (see § 3.2). For the P $\alpha$  line, the  $\text{EW}_{\text{P}\alpha} \approx 4 - 7$  eV (redshifted 3-5 eV) for the observed  $\text{EW}_{\text{H}\alpha}$ .

We now take  $k_B T_{\text{eff}}$  as a free parameter to understand how our results depend on the color correction and spectra. We plot the implied  $n=1$  and total  $N_{\text{Fe}}$  as a function of  $k_B T_{\text{eff}}$  at the observed EW in Figure 7. Since we are interested in Fe at the stopping column (measured from the top of the atmosphere) of

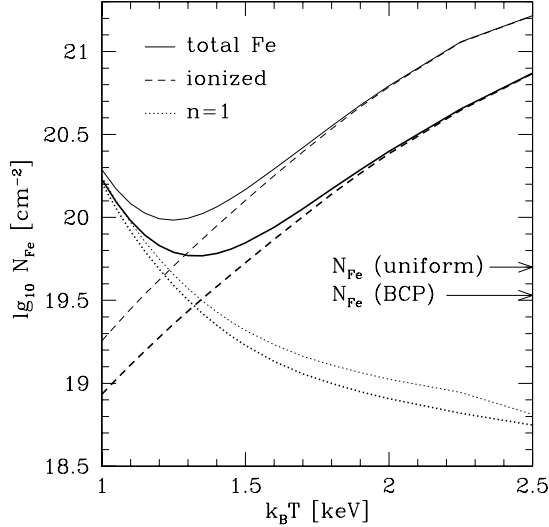


FIG. 7.— The Fe column required to generate the observed EW in the Fe H $\alpha$  line as a function of  $k_B T_{\text{eff}}$  at the Fe stopping column of  $y_{\text{stop}} \approx 1 \text{ g cm}^{-2}$  (thin lines) and  $y_{\text{stop}} = 2 \text{ g cm}^{-2}$  (thick lines), which is more representative of a uniform atmosphere. The various Fe columns represented are the hydrogenic Fe column (dotted-line), fully ionized Fe column (dashed-line) and total Fe column (solid-line). We find that  $N_{\text{Fe}}$  must at least be a factor of 3-4 larger than that predicted from the accretion/spallation scenario of  $3.4 \times 10^{19} \text{ cm}^{-2}$  (BCP), but is within a factor of 2 of a uniform solar metallicity atmosphere of  $5 \times 10^{19} \text{ cm}^{-2}$ .

$y_{\text{stop}} \approx 1 \text{ g cm}^{-2}$  (thin lines), the local proton density, which is important for Stark broadening, is then  $n_p \approx 9.4 \times 10^{22} (k_B T_{\text{eff}}/1 \text{ keV})^{-1} \text{ cm}^{-3}$ . The implied Fe column is minimized at  $k_B T_{\text{eff}} = 1.3 \text{ keV}$ , but it is 3-4 times larger than expected from our solar metallicity accretion/spallation scenario. We also plot a similar Fe column at  $y_{\text{stop}} = 2 \text{ g cm}^{-2}$  (measured from the top of the atmosphere), which is more representative of a uniform atmosphere. From Figure 6 and 7, we find that our the implied Fe column for a solar metallicity atmosphere is within a factor of 3 for the entire range of burst temperatures of 1-2 keV. We discuss these points further in § 4.

### 3.2. Rotational Broadening

Rotational broadening heavily modifies the structure of the lines. We estimate its effects on the line profile as follows. Since the photon occupation number  $n \propto I_\nu/\nu^3$  is invariant under Lorentz transformations, the effect of rotational broadening on the emergent NS flux is

$$F_\nu^{\text{obs}} = \frac{1}{2\pi} \int_0^{2\pi} d\phi \int_0^1 d(\cos \theta) \cos \theta (1 - (\Omega R/c) \sin \theta \cos \phi \sin i)^{-3} I \left( \nu \left( 1 - \frac{\Omega R}{c} \sin \theta \cos \phi \sin i \right), \cos \theta \right), \quad (24)$$

Following various authors (Chandrasekhar 1945), we ignore the effect of Lorentz boosts on the angle and focus on the effects of the frequency shift. We are currently calculating the exact general relativistic calculation elsewhere (Morsink et al. 2005; also see Özel & Psaltis 2003 and Bhattacharyya, Miller & Lamb 2004). In addition

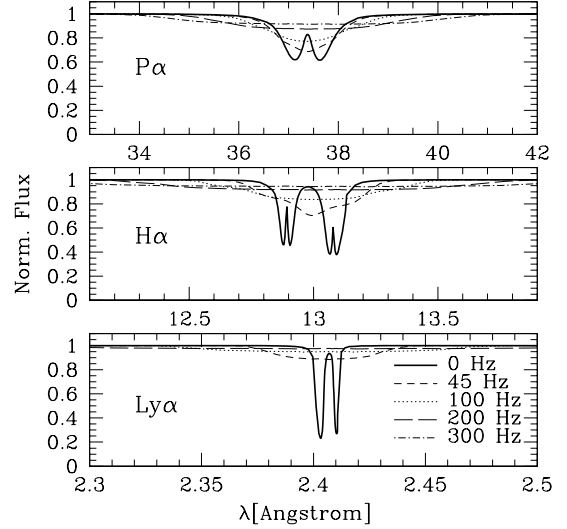


FIG. 8.— Redshifted line profiles for the Fe P $\alpha$ , H $\alpha$ , and Ly $\alpha$  at various rotation rates. We fixed the Fe H $\alpha$  EW to the observed values and assume that the Fe is concentrated in the accretion/spallation stopping layer. We compare models (from bottom to top) at  $\nu_{\text{spin}} \equiv (1+z)^{-1}\Omega/(2\pi) = 0 \text{ Hz}$  (thick-solid lines), 45 Hz (short-dashed lines), 100 Hz (dotted lines), 200 Hz (long-dashed lines), and 300 Hz (dashed-dotted lines) for  $\sin i = 1$ . We do not include a 300 Hz Ly $\alpha$  line profile as it is totally rotationally broadened away.

for narrow lines,  $|(dI_\nu/d \ln \nu)(\Omega R/c)| \gg 1$ , so we can ignore the effects of the  $(1 - \Omega R/c)^3$  in the denominator, leaving

$$F_\nu^{\text{obs}} = \frac{1}{2\pi} \int_0^{2\pi} d\phi \int_0^1 d(\cos \theta) \cos \theta I \left( \nu \left[ 1 - \frac{\Omega R}{c} \sin \theta \cos \phi \sin i \right], \cos \theta \right), \quad (25)$$

showing that rotational line broadening goes like  $(\Omega R/c) \sin i$ . We plot the Fe P $\alpha$ , H $\alpha$  and Ly $\alpha$  lines for a  $1.4 M_\odot$  NS with  $R=9.2 \text{ km}$  at various rotation rates up to 300 Hz in Figure 8. To ease comparison with observation, we plot the lines as a function of wavelength and include the redshift correction of  $z = 0.35$ . We also include the  $1+z$  redshift correction to the rotation rate. For the highest rotation rates ( $> 200 \text{ Hz}$ ), the Fe H $\alpha$  central line depth would only be about 5-10% below the continuum and hence the line would be difficult to detect at the observed EW. At lower rotation rates the doublet nature of the line gives an asymmetric profile with a sharp feature. For the P $\alpha$  line, the fine structure splitting in the line is smaller than the Stark effect so it appears as a singlet.

Rotational broadening is more pronounced on the Ly $\alpha$  transition, which has a FWHM  $\approx 130 \text{ eV}$  at a spin frequency of 45 Hz. This is 5 times larger than the rotational FWHM for the H $\alpha$  line due to the larger energy of the Ly $\alpha$  transition compared to the H $\alpha$  transition. At the implied EW $_{\text{Ly}\alpha}$  matched to the observed EW $_{\text{H}\alpha}$ , the line is extremely shallow with a central line depth of approximately 10%. Hence even at this modest rotation rate, the Ly $\alpha$  line may be difficult to detect. For larger rotation rates ( $> 100 \text{ Hz}$ ), Ly $\alpha$  is so distributed that it may be impossible to detect.

Observations of dips and eclipses on EXO 0748-676

(Parmar et. al. 1986) have revealed that the orbit of the secondary is nearly edge-on ( $\sin i \approx 1$ ). Assuming the rotation axis of the NS is aligned with the orbit, we favor very low rotation rates (50–100 Hz) for EXO 0748-676 compared to the rotation rates that are typically observed in other LMXB systems where the rotation rate is typically 300–600 Hz (for a review see Strohmayer & Bildsten 2003). The recent observation of a 44.7 Hz burst oscillation (Villarreal & Strohmayer 2004) is thus consistent with the observation of the line, assuming that this oscillation is indicative of the NS rotation rate. It raises the exciting prospect of fitting the line with an appropriate spectral calculation to derive the NS radius (Morsink et al. 2005). Other accreting NSs may also possess atomic lines, but we would not expect them to be detected unless they rotate slowly ( $< 100$  Hz) or are highly inclined.

### 3.3. Radiative Levitation

BCP noted that Fe in the atmosphere may be sustained by radiative levitation similar to what occurs in hot stars (Michaud 1970; Michaud et al. 1976) and white dwarfs (Vauclair, Vauclair & Greenstein 1979; Vennes et al. 1988; Chayer, Fontaine & Wesemael 1995). To begin, we calculate the radiative force on a hydrogenic Fe atom,  $F_{\text{rad}} = c^{-1} \int \sigma_{\nu} F_{\nu} d\nu$ , from reflection of the incident flux,  $F_{\nu}$ , where  $\sigma_{\nu}$  is the cross section and is defined as  $\sigma_{\nu} = \sigma_{0,12} \phi_{\nu}$ ,  $\sigma_{0,12} = \pi e^2 f_{12} / (m_e c \Delta\nu)$ ,  $\phi_{\nu}$  is the convoluted Holtsmark profile, and  $f_{12} = 0.42$  is the oscillator strength for the Ly $\alpha$  transition (Bethe & Salpeter 1957). Assuming that the flux does not change as we integrate across the line,  $\int \sigma_{\nu} F_{\nu} d\nu = F_{\nu} \pi e^2 f_{12} / (m_e c)$ . For a radiation field that is isotropic in the outward hemisphere,  $F_{\nu} = \pi B_{\nu}(T)$  (Rybicki & Lightman 1979),  $B_{\nu}(T)$  is the Planck function which we approximate with the Wien tail, we find.

$$\frac{F_{\text{rad}}}{Am_p g} \approx 9 \times 10^3 \exp\left(-\frac{6.9 \text{ keV}}{k_B T_{\text{eff}}}\right) A_{56}^{-1} g_{14}^{-1}, \quad (26)$$

where  $g_{14} = g/10^{14} \text{ cm s}^{-2}$ . For  $k_B T_{\text{eff}} = 1 \text{ keV}$ , the radiation force on the Ly $\alpha$  exceeds gravity by a factor of 9 if all the Fe is hydrogenic.

Since the radiation force exceeds that of gravity, the Fe will not necessarily sediment. Rather, Fe can be sustained in the atmosphere, allowing for a potential concentration. As the column of Fe builds, more and more of the line flux is absorbed which decreases the radiative force. This continues until an equilibrium column is reached where enough of the line flux is absorbed that the Fe feels the same net force as a background proton, so that both species have the same scale height (Chayer, Fontaine & Wesemael 1995). This is achieved when the radiative force is equal to the effective force  $F_{\text{rad}} = Am_p g_{\text{eff}} = [A - (Z + 1)/2] m_p g$ , which takes into account the effects of both gravity and the electric field for a hydrogen atmosphere and assumes all the Fe is hydrogenic (Vennes et al. 1988; Chayer, Fontaine & Wesemael 1995).

We now estimate the equilibrium column sitting above the continuum photosphere. The radiative force on a scattering layer is

$$F_{\text{rad}} = \sum_{\text{lines}} \frac{F_{\nu_i, \text{cont}} EW_i}{c}, \quad (27)$$

where  $\nu_i$  is the energy of the  $i$ th line,  $F_{\nu_i, \text{cont}}$  is the continuum flux and  $EW_i$  is the equivalent width of the  $i$ th line. For pure coherent scattering, Schuster's law (eq.[20]) and the definition of the equivalent width (eq.[23]) gives

$$EW_i = \int \frac{\tau_{0,i}^{\text{tot}} \phi_{\nu,i}}{2/\sqrt{3} + \tau_{0,i}^{\text{tot}} \phi_{\nu,i}} d\nu, \quad (28)$$

where  $\tau_{0,i}^{\text{tot}}$  and  $\phi_{\nu,i}$  is the normalization of the optical depth and line profile distribution of the  $i$ th line respectively. We find an extremely simple form for equation (28) by taking the asymptotic form<sup>3</sup> of the Holtsmark distribution  $\phi_{\nu} \approx 0.75 (|\nu - \nu_0|/\Delta\nu_{\text{Stark}})^{-2.5}$ . Assuming  $\tau_0^{\text{tot}}$  is large, we break up the integral in equation (28) into a regime where  $\tau_0^{\text{tot}} \phi_{\nu}$  is large compared to  $2/\sqrt{3}$  and a regime where  $\tau_0^{\text{tot}} \phi_{\nu}$  is small compared to  $2/\sqrt{3}$ . Thus, we get

$$EW_i \approx 2\tau_{0,i}^{\text{tot}} \Delta\nu_{\text{Stark}} \left[ \int_0^{\eta_0} \frac{d\eta}{\tau_0^{\text{tot}}} + \int_{\eta_0}^{\infty} \frac{0.75\eta^{-2.5}}{2/\sqrt{3}} d\eta \right], \\ \approx 2.8 \Delta\nu_{\text{Stark}} (\tau_{0,i}^{\text{tot}})^{0.4} \quad (29)$$

where  $\eta = |\nu - \nu_0|/\Delta\nu_{\text{Stark}}$  and  $0.75\tau_0^{\text{tot}}\eta_0^{-2.5} = 2/\sqrt{3}$ . We extend this simple form for the EW to handle fine structure splitting if the split lines are widely separated and therefore distinct. We sum over each split line to get

$$EW_i \approx 2.8 \Delta\nu_{\text{Stark}} (\tau_{0,i}^{\text{tot}})^{0.4} \sum_j s_{i,j}^{0.4}, \quad (30)$$

where  $s_{i,j}$  are the relative strength of each split line for the  $i$ th transition. For Ly $\alpha$ , which is split into two lines with a ratio of 2:1, we find  $EW_{\text{Ly}\alpha} = 4.2 \Delta\nu_{\text{Stark, Ly}\alpha} (\tau_{0, \text{Ly}\alpha}^{\text{tot}})^{0.4}$ . Similarly for H $\alpha$  with a line strength ratio of 9:1:5,  $EW_{\text{H}\alpha} = 5.2 \Delta\nu_{\text{Stark, H}\alpha} (\tau_{0, \text{H}\alpha}^{\text{tot}})^{0.4}$ .

Following our previous discussion, we now equate the radiative force (eq.[27]) to the effective force to find the equilibrium column. For simplicity, let us first consider only the Ly $\alpha$  line and a radiation field that is isotropic in the outer half hemisphere. We find

$$N_{\text{Fe, tot}} \approx 5 \times 10^{20} \left( \frac{g}{3 \times 10^{14} \text{ cm s}^{-2}} \right)^{5/3} \xi^{-2/3} \text{ cm}^{-2}, \quad (31)$$

for  $kT \approx 2 \text{ keV}$ , where  $\xi \equiv N_{\text{Fe, tot}}/N_{\text{Fe, n=1}}$  is the ratio of total Fe column to ground state hydrogenic Fe column. The Ly $\alpha$  equivalent width that is associated with this Fe column is

$$EW_{\text{Ly}\alpha} \approx 400 \left( \frac{g}{3 \times 10^{14} \text{ cm s}^{-2}} \right)^{2/3} \xi^{-2/3} \text{ eV}. \quad (32)$$

Radiative levitation can easily sustain an atmosphere whose metallicity can be supersolar. In Saha equilibrium, the ratio between fully ionized Fe and the n=1 hydrogenic state is 10-20 and  $N_{\text{Fe, tot}} = 7 - 12 \times 10^{19} \text{ cm}^{-3}$ , larger than a constant solar metallicity atmosphere

<sup>3</sup> The standard definition is  $\phi_{\nu} \approx 1.5 (|\nu - \nu_0|/\Delta\nu_{\text{Stark}})^{-2.5}$  for large  $(|\nu - \nu_0|/\Delta\nu_{\text{Stark}})$ . The numerical prefactor of 0.75 comes from the fact that the line is symmetric and hence the distribution runs from  $-\infty$  to  $\infty$  and not from 0 to  $\infty$



$N_{\text{Fe}} \approx 5 \times 10^{19} \text{ cm}^{-2}$  (BCP). These values are also tantalizingly close to what would be required for the measured  $\text{H}\alpha$  line, but we note that the radiatively levitated Fe column is sensitively dependent on the background continuum and surface gravity. Since bursting NS atmospheres are expected to be harder than a blackbody as discussed earlier in § 2, we would expect these values to be lower limits. The associated  $\text{Ly}\alpha$  EW for these Fe columns in this approximation is 50-90 eV.

Other transitions also contribute to the radiative force on the Fe column. We now show that their contributions are small compared to the  $\text{Ly}\alpha$  radiative force. First, we consider the contribution from the  $\text{H}\alpha$  transition. For a Boltzmann distribution between the  $n=1$  and the  $n=2$  state at  $kT = 2 \text{ keV}$ , the column density in the  $n=2$  state is  $N_{\text{Fe},n=2} = 0.1 N_{\text{Fe},n=1}$ . The radiative force from the  $\text{H}\alpha$  transition is  $F_{\text{rad},\text{H}\alpha} \approx 2 \times 10^{12} \text{ g cm s}^{-2}$  which is a factor of 5 smaller than the radiative force on the  $\text{Ly}\alpha$  transition of  $F_{\text{rad},\text{Ly}\alpha} \approx 10^{13} \text{ g cm s}^{-2}$ . The contribution from the  $\text{H}\alpha$  transition increases the column by about a third, but we will ignore this contribution in keeping with the order of magnitude spirit of this calculation. Other transitions also contribute, but their radiative forces are weaker as their fluxes are weaker by the Rayleigh-Jeans factor of  $\nu^2$  compared to  $\text{H}\alpha$ .

#### 4. DISCUSSION AND CONCLUSIONS

Motivated by the accretion/spallation scenario that we first presented in BCP, we have calculated the resonant radiative transfer of a thin scattering layer above the NS photosphere. While our calculation and microphysics are geared toward understanding the feature as an Fe  $\text{H}\alpha$  line, the basic physics would remain the same for other atomic transitions. Namely, if the line is produced near the continuum photosphere where the densities are relatively high, Stark broadening is dominant, NLTE effects are prevalent and the line is a result of resonant scattering. Applied to Fe  $\text{H}\alpha$ , our calculations show that the EW of the Fe  $\text{H}\alpha$  line observed by CPM from EXO 0748-676 requires an Fe column 3-10 times larger than the accretion/spallation scenario predicts for accretion of solar metallicity material (BCP). We also approximate a uniform solar metallicity atmosphere by assuming the Fe sits at a larger depth. In this case, we find that the required column of Fe is within a factor of 3 of a solar metallicity atmosphere over a large range of temperatures.

The fact that the  $\text{H}\alpha$  line is narrow requires that the rotation rate of EXO 0748-676 is slow. Larger spin rates, assuming a neutron star radius of around 10 km, would wash out such a line unless the surface emission is confined to a narrow region around the spin axis (Bhattacharyya, Miller & Lamb 2004). A slow rotation rate for EXO 0748-676 is consistent with the recently measured 44.7 Hz burst oscillation (Villarreal & Strohmayer 2004). With these line profiles in hand and assuming that the burst oscillation of 44.7 Hz is the rotation rate of the NS, detailed fits to the data raises the exciting prospect of fitting for the neutron star radius (Morsink et al. 2005).

Since the fine structure splitting of Fe  $\text{H}\alpha$  is of order the size of the rotational broadening, we cannot assume that the line is narrow compared to the rotational broadening. Previous work (Özel & Psaltis 2003; Bhattacharyya,

Miller & Lamb 2004) has presumed that the intrinsic line profile does not matter because rotational broadening is dominant. While true for NS rotating at 300-600 Hz, it is not the case for a Fe  $\text{H}\alpha$  line at 45 Hz for a 10 km NS. Rotational broadening may be the largest effect, but it is by no means the dominant effect. Therefore, the intrinsic line profile must be known to apply the observed lines to the study of NS physics.

We also estimated that the Fe  $\text{EW}_{\text{Ly}\alpha}$  and  $\text{EW}_{\text{P}\alpha}$  are approximately 15-20 eV and 3-7 eV respectively at the observed  $\text{EW}_{\text{H}\alpha}$ . We can extend this calculation to include other  $n=1$  and  $n=2$  transitions aside from  $\text{Ly}\alpha$  and  $\text{H}\alpha$ . However, because of the greatly reduced oscillator strengths, these lines are significantly weaker. For instance, we have modeled  $\text{H}\beta$  EW to be  $< 2 \text{ eV}$ . Rotational broadening makes a huge impact on the observability of the Fe  $\text{Ly}\alpha$  transition. While the spectral resolution of Chandra and Astro E2 is more than adequate to detect such a line, the  $\text{Ly}\alpha$  line will be shallow and difficult to detect. We expect rotational broadening to be a small effect for  $\text{P}\alpha$ , however, the redshifted energy of the  $\text{P}\alpha$  transition of 330 eV would make it difficult due to interstellar absorption.

In calculating these profiles of Stark broadened lines, we have assumed a pure hydrogen atmosphere. However, the Stark broadening scale given in equation (3) depends on the background composition. Namely  $\Delta E_{\text{Stark}} \propto (2A/(Z+1))^{2/3} Z^{1/3}$ . For solar composition,  $\Delta E_{\text{Stark}}$  is larger by 14%. This reduces the required  $N_{\text{Fe}}$  needed to reproduced the observed EW by 10%. For a pure He atmosphere  $\Delta E_{\text{Stark}}$  is larger by a factor of 2.42, which reduces the required  $N_{\text{Fe}}$  to reproduce the observed EW by 60%. For an atmosphere that consist of equal parts He and H by number, we find the required  $N_{\text{Fe}}$  is reduced by about 50%. Such He-rich atmosphere would demand accretion from a H-poor donor such as 4U 1820-30, but the initial spallation would reduce the He fraction at the photosphere.

The formation of the He-like Fe spectral feature in the low-temperature part of the burst is an issue that warrants further study. In Saha equilibrium, H-like Fe transitions to He-like Fe at 1.2 keV (CPM). We note however that the microphysics of this line is significantly different from the  $\text{H}\alpha$  line. Its intrinsic broadening is due to thermal Doppler effects because the lack of degenerate opposite parity states suppresses the linear Stark effect (Bethe & Salpeter 1957). Modeling this feature requires a separate calculation which is beyond the scope of this paper.

If accretion/spallation is indeed not the endpoint of accretion onto a neutron star, we expand on radiative levitation as a means to suspend the Fe, which we first pointed out in BCP. We give a simple estimate for the Fe column that could be suspended by radiative levitation. We find that radiative levitation could suspend a column of Fe needed to produce the line. However, this result depends sensitively on the exact nature of the background spectra. Further work will be necessary as the continuum spectra could be much harder than the blackbody background that we have assumed.

Though we assume solar metallicity throughout our calculations, the composition of the accreting material remains highly uncertain. If the metallicity of the flow is

sufficiently supersolar, the disparity between the accretion/spallation Fe column and that implied from observation can be resolved. However, the contrast between the deep dips and the unobscured state of EXO 0748-676 indicates that the metallicity may be subsolar by a factor of 2-7 (Parmar et al. 1986). More recent work has found that the abundance ratios of Mg, Ne and O are consistent with solar with large uncertainties (Jimenez-Garate, Schulz & Marshall 2003). The intrinsic metallicity of the flow remains largely uncertain.

We thank the anonymous referee and Deepto Chakrabarty for a careful reading of our manuscript. Their comments greatly clarified this work. We thank

R. Sunyaev for detailed discussions and for highlighting the importance of the fine structure splitting for high Z elements. We thank S. W. Davis for discussions on numerical solutions to radiative transfer problems. This work was supported by the National Science Foundation (NSF) under PHY 99-07949, and by the Joint Institute for Nuclear Astrophysics through NSF grant PHY 02-16783. Support for this work was also provided by NASA through Chandra Award Number GO4-5045C issued by the Chandra X-ray Observatory Center, which is operated by the SAO for and on behalf of NASA under contract NAS8-03060. I.W. receives partial support from NSF grant AST-0307273.

#### REFERENCES

- Arav, N. 1996, ApJ, 465, 617  
 Bhattacharyya, S., Miller, M. C. & Lamb. F. K. 2004, submitted to ApJ Letters, astro-ph/0412107  
 Bethe, H. A. & Salpeter, E. E. 1957 *Quantum Mechanics of One- and Two-Electron Atoms* (Berlin: Springer-Verlag)  
 Bildsten, L., Chang, P. & Paerels, F. 2003, ApJ, 591, L29 (BCP)  
 Bildsten, L., Salpeter, E. E. & Wasserman, I. 1992, ApJ, 384, 143  
 Castor, J. I. 1974, ApJ, 189, 273  
 Chandrasekhar, S. 1945, Rev. Mod. Phys., 17, 138  
 Chayer, P., Fontaine, G., Wesemael, F. 1995, ApJS, 99, 189  
 Cottam, J., Paerels, F. & Mendez, M. 2002, Nature, 420, 51 (CPM)  
 Day, C. S. R., Fabian, A. C. & Ross, R. R. 1992, MNRAS, 257, 471  
 Foster, A. J., Ross, R. R., & Fabian, A. C. 1987, MNRAS, 228, 259  
 Gottwald, M., Haberl, F., Parmar, A. N., & White, N. E. 1986, ApJ, 308, 213  
 Gray, D. F. 1992, *The Observation and Analysis of Stellar Photospheres* (Cambridge: Cambridge University Press)  
 Harrington, J. P. 1973, MNRAS, 162, 43  
 Jefferies, J. T. 1968 *Spectral Line Formation* (Waltham: Blaisdell)  
 Jimenez-Garate, M. A., Schulz, N. S. & Marshall, H. L. 2003, ApJ, 590, 432  
 Joss, P. C. 1977, Nature, 270, 310  
 Kuulkers, E., Homan, J., van der Klis, M., Lewin, W. H. G., & Mendez, M. 2002, A&A, 382, 947  
 Lewin, W. H. G., van Paradijs, J., & Taam, R. E. 1993, Space Sci. Rev., 62, 233  
 London, R. A., Taam, R. E. & Howard, W. M. 1986, ApJ, 306, 170  
 Madej, J. 1974, Acta. Astron., 24, 327  
 Madej, J. 1991, ApJ, 376, 161  
 Madej, J., Joss, P. C. & Rozanska, A. 2004, ApJ, 602, 904  
 Magnier, E., Lewin, W. H. G., van Paradijs, J., Tan, J., Penninx, W. & Damen, E. 1989, MNRAS, 237, 729  
 Michaud, G. 1970, ApJ, 160, 641  
 Michaud, G., Charland, Y., Vauclair, S., & Vauclair, G. 1970, ApJ, 210, 447  
 Mihalas, D. 1978, *Stellar Atmospheres* (San Francisco: W. H. Freeman)  
 Morsink, S. M., Chang, P., Bildsten, L. & Wasserman, I. 2005, in prep.  
 Nakamura, N., Inoue, H. & Tanaka, Y. 1988, PASJ, 40, 209  
 Özel, F., & Psaltis, D. 2003, ApJ, 582, L31  
 Paerels, F. 1997, ApJ, 476, L47  
 Parmar, A. N., White, N. E., Giommi, P. & Gottwald, M. 1986, ApJ, 308, 199  
 Pavlov, G. G., Shibanov, Y. A., & Zavlin, V. E. 1991, MNRAS, 253, 193  
 Potekhin, A. Y., Chabrier, G. & Gilles, D. 2002, Phys. Rev. E, 65, 036412  
 Rybicki, G. B. & Lightman, A. P. 1979 *Radiative Processes in Astrophysics* (New York: Wiley)  
 Schuster, A. 1905, ApJ, 21, 1  
 Strohmayer, T. & Bildsten, L. 2004, to appear in Compact Stellar X-ray Sources, ed. W.H.G. Lewin & M. van der Klis, (Cambridge University Press: London) astro-ph/0301544  
 Turner, M. J. L. & Breedon, L. M. 1984, MNRAS, 208, 29p  
 van Paradijs, J. 1982, A&A, 107, 51  
 Vauclair, G., Vauclair, S., & Greenstein, J. L. 1979, A&A, 80, 79  
 Vennes, S., Pelletier, C., Fontaine, G., & Wesemael, F. 1988, ApJ, 331, 876  
 Villarreal, A. R. & Strohmayer, T. E. 2004, ApJ, 614, L121  
 Waki, I. et al. 1984, PASJ, 36, 819  
 Zel'dovich, Ya. & Shakura, N. 1969, Soviet Astron, 13, 175